



# Mechanical and tribological properties of nanocomposite TiSiN coatings

Y.H. Cheng<sup>a,\*</sup>, T. Browne<sup>a</sup>, B. Heckerman<sup>a</sup>, E.I. Meletis<sup>b</sup>

<sup>a</sup> American Eagle Instruments, Inc., 6575 Butler Creek Rd, Missoula, MT 59808, United States

<sup>b</sup> Department of Materials Science and Engineering, University of Texas at Arlington, Arlington, TX 76019, United States

## ARTICLE INFO

### Article history:

Received 28 May 2009

Accepted in revised form 24 November 2009

Available online 1 December 2009

### Keywords:

Filtered cathodic arc  
Nanocomposite coating  
Mechanical property  
Wear property  
Adhesion wear  
Abrasive wear

## ABSTRACT

TiSiN coatings with a thickness of 2.5  $\mu\text{m}$  were deposited using a Large Area Filtered Arc Deposition (LAFAD) technique with TiSi targets having different Si content. The influence of the Si content in the coatings on the mechanical properties and tribological behaviors of the TiSiN coatings were systematically studied using nanoindentation and a pin-on-disk tribometer. Nanoindentation results show that the hardness and Young's modulus of the TiSiN coatings increase with increasing Si content in the coatings. Wear test results indicate that the wear rate and friction coefficient of the 440a stainless steel coupons were significantly reduced by deposition of the TiSiN coatings, and the tribological behaviors of the TiSiN coatings are strongly dependent on the Si content in the coatings and the testing ball material. TiSiN coatings exhibit similar friction coefficient when tested against  $\text{Al}_2\text{O}_3$  and 302 stainless steel balls, but increasing Si content in the coatings causes an increase in the friction coefficient of the TiSiN coatings. With the increase in the Si content in the coatings, the wear rate of the TiSiN coatings decreases when tested against  $\text{Al}_2\text{O}_3$  balls, but increases significantly when tested against 302 stainless steel balls. The capability of forming a transfer layer on the ball surface contributes to the change in the friction coefficient and wear rate with Si content in the coating and ball materials.

© 2009 Elsevier B.V. All rights reserved.

## 1. Introduction

Nanocomposite TiSiN coatings, consisting of nanosized TiN grains embedded in amorphous SiN matrix with atomic thickness, have gained considerable attention in the last decade due to their extremely high indentation hardness (40–80 GPa) [1–7], excellent high temperature oxidation resistance [8,9], and high abrasion and erosion resistance [10,11]. Various deposition techniques, such as Chemical Vapor Deposition (CVD) [8,12,13], Plasma Enhanced Chemical Vapor Deposition (PECVD) [14], Magnetron Sputtering [15–17], and Cathodic Vacuum Arc [18–20], have been utilized to deposit TiSiN coatings. It has been proposed that super-hard nanocomposite TiSiN coatings could only be deposited at high deposition temperature (>500 °C) and high nitrogen partial pressure (>1 Pa) [1–3]. However, our preliminary results show that super-hard (>50 GPa) nanocomposite TiSiN coatings could successfully be deposited at a low temperature of 350 °C and a low nitrogen pressure of 0.02 Pa by our patented Large Area Filtered Arc Deposition (LAFAD) technology due to the high ion energy and high ionization rate [21].

Si content in the TiSiN coatings is an important factor that significantly affects structure and mechanical properties, as well as the tribological behavior of the coatings [1–4,16,22,23]. Generally, with increasing Si content in the TiSiN coatings up to 7–12 atomic

percentage (at.%), the TiN grain size decreases to a few nm and the internal stress, hardness, and Young's modulus increase remarkably to a maximum. Further increase in the Si content in the coating causes a reduction in the internal stress, hardness and Young's modulus. However, the reported tribological behaviors of the TiSiN coatings have been significantly different and even controversial. When wear tested against steel balls, with an increase in Si content in the TiSiN coatings, Ma et al. [22] found an increase in the friction coefficient and a reduction in the wear rate; K.H. Kim et al. [24] reported a decrease in the friction coefficient; S.H. Kim et al. [16] found a reduction in friction coefficient and an increase in the wear rate; and Patscheider et al. [25] reported an increase in hardness, wear rate, and friction coefficient.

In this study, a LAFAD-1 system was used to deposit TiSiN coatings with different Si content by using TiSi alloy targets with different Si/Ti ratio. The influence of the Si content in the coatings on the hardness, Young's modulus, friction coefficient and wear resistance of the TiSiN nanocomposite coatings on 316 and 440a stainless steel substrates were systematically studied.

## 2. Experiment

A LAFAD surface engineering system (LAFAD-1) was used to deposit TiSiN nanocomposite coatings. The detailed description of this deposition system was reported previously [26]. Briefly, this system consists of one dual filtered arc source, one rectangular plasma-guide chamber, one deposition chamber, auxiliary anodes, heating system, substrate bias system, and vacuum system. The dual filtered arc

\* Corresponding author.

E-mail addresses: [yh\\_cheng@yahoo.com](mailto:yh_cheng@yahoo.com), [ycheng@am-eagle.com](mailto:ycheng@am-eagle.com) (Y.H. Cheng).

source consists of two primary cathodic arc sources utilizing round TiSi targets, which are placed opposite to each other on the side walls of the plasma-guide chamber, surrounded by rectangular deflecting coils, and separated by an anodic baffle plate. The deposition temperature was controlled by heating elements and measured by a thermal couple located on top of the deposition chamber. The deposition zone for this system is approximately 500 mm in diameter  $\times$  300 mm high. 316 and 440a stainless steel coupons were used as the substrate for characterizing the wear resistance of the nanocomposite coatings. Stainless steel coupons were cut from  $\phi$ 18.75 mm  $\times$  300 mm bars, and then sent to Lap-Rite Ind., Inc. (IL, USA) for grinding and polishing. The coupons were first lapped to a roughness of about 2  $\mu$ m by using alumina slurry with a size of 17  $\mu$ m. Then the lapped coupons were polished using diamond slurry with a size of 1  $\mu$ m to a mirror finished surface with a surface roughness (RMS) of about 12 nm.

The substrates were ultrasonically cleaned and then dried before being loaded into the deposition chamber. Before deposition, the coupons were subjected to Ar arc plasma cleaning at a pressure, temperature, bias, and time of 0.08 Pa, 350  $^{\circ}$ C,  $-$ 250 V, and 15 min, respectively, followed by the TiSi ion subplantation at a pressure, bias, and time of 0.02 Pa, 500 V, and 2 min, respectively. During the Ar plasma cleaning, the arc plasma was turned on, but the deflection magnetic field was turned off, which allow only electrons getting into the chamber and ionize the Ar gas and forms dense plasma. After Ar plasma cleaning, deflection magnetic field was turned on, Ti and Si ions were guided into the deposition chamber, which were used to do subplantation and coating deposition. In order to improve the adhesion of the TiSiN coatings, a TiSi–TiSiN gradient multilayer with a thickness of about 200 nm was deposited onto the coupon surface. The gradient layer was deposited by gradually increasing N<sub>2</sub> fraction in the mixed Ar and N<sub>2</sub> gases from 0 to 100%. Following the deposition of the gradient layer, TiSiN coatings with a thickness of 2.5  $\mu$ m were deposited.

TiSi alloy targets with Si content of 5, 10, 15, and 20 at.% were used to deposit TiSiN coatings, which are referred to as TiSi5N, TiSi10N, TiSi15N, and TiSi20N, respectively. The deposition parameters for TiSiN coatings were: deposition pressure, 0.02 Pa; substrate bias,  $-$ 40 V; and deposition temperature, 350  $^{\circ}$ C. The Si content in the coatings was measured by using X-ray photoelectron spectroscopy (XPS) method. The corresponding Si content in the TiSi5N, TiSi10N, TiSi15N, and TiSi20N coatings is 0.5, 1.4, 4.9, and 7.7 at.%, respectively [15].

Nanoindentation tests were conducted using a MTS nano Indenter<sup>®</sup> XP (MTS Systems Corp., Oak Ridge, TN, USA) with a Berkovich diamond tip. Hardness and elastic modulus were measured using the continuous stiffness measurement (CSM) option. Si was used as a standard sample for the initial calibration. A conventional ball-on-disk wear tester was used to characterize the dry friction and wear performance of the TiSiN coatings coated and as-received 440a stainless steel coupons. The tribological tests were performed using a pin-on-disk wear tester (TRB) from CSM Instruments at a load of 1 N and sliding distance of 300 m. During testing, 302 stainless steel and alumina balls with a diameter of 6 mm were used as counter materials. The wear loss of different samples was measured by a surface profilometer (Veeco Dektak8) scanning across the wear track. The stylus radius and stylus force were set to 5  $\mu$ m and 10 mg, respectively. The friction coefficient was determined as a function of sliding distance. Wear morphology was observed using a Hitachi S-4700 field emission Scanning Electron Microscopy (SEM) operated at 20 kV.

### 3. Results

The hardness and Young's modulus of the TiSiN nanocomposite coatings on 316 stainless steel substrates were measured by using

CSM method. To eliminate the influence of the soft steel substrate on the measured hardness and Young's modulus, the hardness and Young's modulus values in the indentation depth range of 5–10% coating thickness were averaged. These were regarded as the effective hardness and Young's modulus of the TiSiN nanocomposite coatings. Fig. 1 illustrates the dependence of the hardness and modulus of the coatings deposited on 316 stainless steel coupons on the Si content in the coatings. As shown, the hardness and Young's modulus of the TiSiN coatings increases continuously from 36 GPa and 406 GPa to 51 GPa and 449 GPa, respectively, with increasing Si content in the coatings from 0.5 to 7.7 at.%.

The X-ray diffraction (XRD) and XPS results [27] show that the TiSiN coatings deposited by LAFAD is comprised of nanocrystalline TiN and amorphous S<sub>3</sub>N<sub>4</sub>; the content of the amorphous Si<sub>3</sub>N<sub>4</sub> phase increases with increasing Si content in the coatings; and the increase in the Si content in the coatings from 0.5 to 4.5 at.% results in a linear decrease in the grain size from 14.9 to 5.4 nm. Further increase in the Si content to 7.7 at.% leads to a slight increase in the grain size to 5.8 nm. As hardness is a measure of the resistance of materials to local plastic deformation, it is directly correlated to the nucleation and slipping of dislocation. It is well accepted that small grains typically have lower dislocation density, and the decrease in grain size leads to an increase in the grain boundary, which acts as obstacles to dislocation flow across grains. The combined effects of low dislocation density and larger grain boundary area contribute to the decrease in the hardness and modulus with increasing Si content in the coatings. For the coatings with high Si content, the grain size reduced to below 6 nm. In this case, the dislocations are absent in the grains and the plastic deformation mechanism changes from dislocation sliding to grain boundary sliding. However, the high bonding energy of Si–N and Si–Ti bonds in the grain boundary resisted the grain sliding, resulting in the super high hardness of the TiSiN coatings.

The friction and wear properties of the TiSiN coatings were investigated by a pin-on-disk test. Both 302 stainless steel and Al<sub>2</sub>O<sub>3</sub> balls were used as counterparts. Fig. 2 shows the typical friction coefficient vs. the sliding distance curves of the uncoated 440a coupons and TiSiN nanocomposite coatings coated 440a stainless steel coupons tested at a load of 1 N with a total sliding distance of 300 m, against (a) Al<sub>2</sub>O<sub>3</sub> ball and (b) 302 stainless steel balls.

All friction coefficients vs. wear distance curves exhibit two stages, running-in stage and steady-state stage. In the running-in stage, the friction coefficient increases with increasing sliding distance. While in the steady-state stage, all the curves are smooth and constant. When Al<sub>2</sub>O<sub>3</sub> balls were used, the sliding distances at the running-in stage increased with increasing Si content in the coatings, while the curves at the steady-state stage are flat. As shown in Fig. 2b, when 302 stainless steel balls were used, large variations of the friction

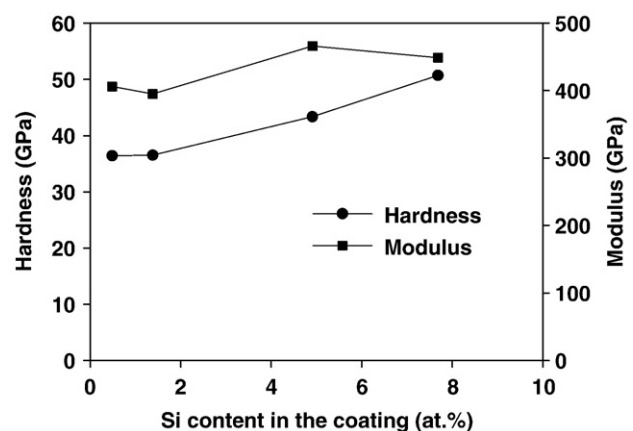


Fig. 1. Dependence of the hardness and modulus of the coatings on the Si content in the coatings.

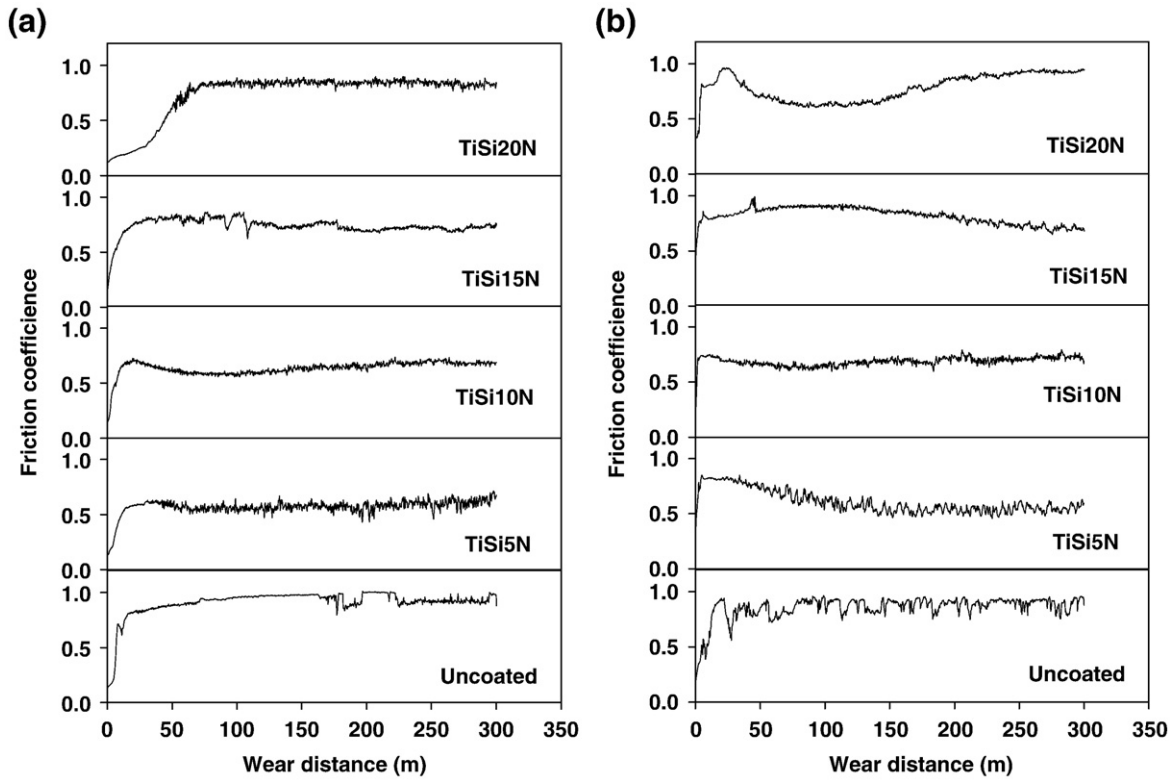


Fig. 2. Typical friction coefficient vs. sliding distance curves of the uncoated and TiSi5N, TiSi10N, TiSi15N, and TiSi20N coated 440a stainless steel coupons tested against (a)  $Al_2O_3$  and (b) 302 stainless steel balls.

coefficient with wear distance were observed for the uncoated stainless steel coupons. Fig. 3 summarizes the friction coefficient of TiSiN coatings wear against  $Al_2O_3$  and 302 stainless steel balls at the steady-state as a function of the Si content in the coatings. The long dash line and the dotted line show the friction coefficient of the uncoated 440a coupons against  $Al_2O_3$  and 302 stainless steel balls, respectively. As shown, when tested against  $Al_2O_3$  and 302 stainless steel balls, the uncoated 440a stainless steel possesses the highest and similar friction coefficient. It is interesting to note that the friction coefficient for each TiSiN coating is almost the same when different ball materials were used. With the increase in the Si content in the coatings from 0.5 to 7.7 at.%, the friction coefficient increases gradually from 0.6 to 0.9.

Fig. 4 illustrates the typical 3D images of the wear track on the uncoated, TiSi10N, TiSi15N, and TiSi20N coated 440a steel coupons

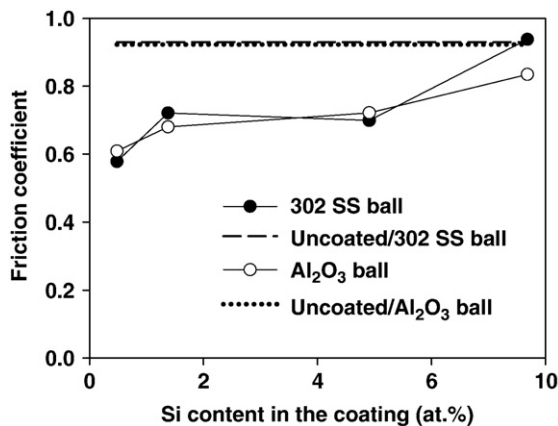
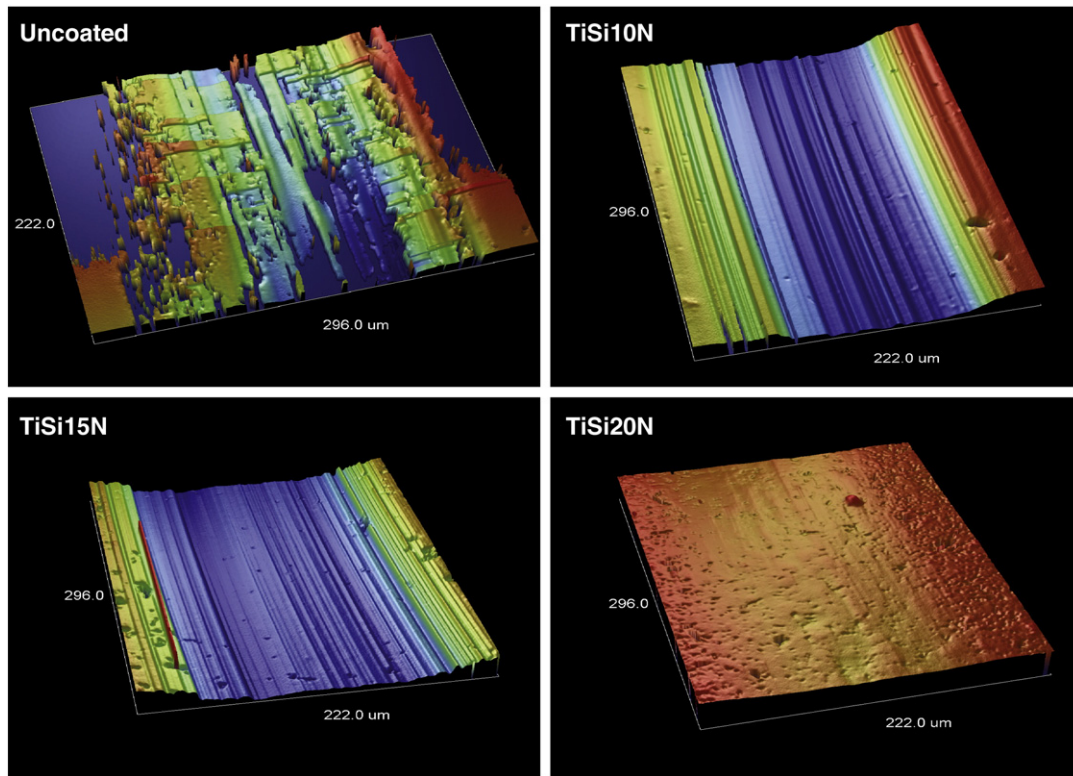


Fig. 3. Friction coefficient of TiSiN coatings against  $Al_2O_3$  and 302 stainless steel balls as a function of Si content in the coatings.

tested against  $Al_2O_3$  ball at 1 N and 300 m. The 3D images taken by a profilometer show deep and wide wear tracks on the uncoated 440a coupon surface. The high magnification SEM observation exhibits plastic deformation of the top layer in the wear track caused by shear force. On the wear track of TiSiN coated coupons, fine abrasion wear grooves appeared on the 3D images, indicating that the wear mechanism for TiSiN coatings against  $Al_2O_3$  balls is abrasive wear. In addition, large debris particles were observed in the wear track, which act as abrasive wear media during wear testing, leading to the formation of wear grooves. With the increase in the Si content in the coatings, the wear track becomes shallower and smoother. For the TiSi20N coatings, the wear track is so smooth that no signs of wear were seen on the 3D images, indicating excellent wear resistance of the coatings.

The typical 3D images of the wear track on the uncoated, TiSi10N, TiSi15N, and TiSi20N coated 440a steel coupons tested against 302 stainless steel balls at 1 N and 300 m are shown in Fig. 5. On the uncoated 440a stainless steel coupon, the wear track is very rough and wide. 3D images show clearly some extrusions on the wear track surface indicating an adhesion wear mechanism. Deep grooves along the sliding direction were observed on the wear track of all TiSiN coatings. In addition, extrusions were also observed in some areas of the high magnification 3D images of the TiSiN coatings with low Si content. This implies that for TiSiN coatings with lower Si content, the wear mechanism is a combination of adhesion and abrasion, but the wear mechanism for the TiSi20N coating is abrasion wear.

To compare the depth of the wear track, the 2D wear track profiles on the uncoated and TiSiN coated coupons against  $Al_2O_3$  and 302 stainless steel balls are plotted in Fig. 6a and b, respectively. It is worth pointing out that the scale of the Y-axis in Fig. 6a for the coated disk is only half of the uncoated disk. For the uncoated 440a coupons, the wear track is very deep (about  $2 \mu m$ ) and wide ( $200 \mu m$ ). The wear track surface is very rough, indicating low wear resistance of the uncoated 440a stainless steel substrate. The coating of 440a coupons



**Fig. 4.** Typical 3D images of the wear track on the uncoated, TiSi5N, TiSi10N, and TiSi20N coated 440a steel coupons tested against  $\text{Al}_2\text{O}_3$  ball at 1 N and 300 m.

with TiSi5N results in a drastic decrease in the depth and width of the wear track to  $0.8\ \mu\text{m}$  and  $160\ \mu\text{m}$ , respectively. For the TiSi10N coatings, although some deep grooves ( $1\ \mu\text{m}$ ) were observed, the average depth of the wear track reduces to about  $0.6\ \mu\text{m}$ . There is no

significant change in the wear width. With the increase of Si content in the targets to 15 and 20 at.%, the depth of the wear track reduces to below  $0.4$  and  $0.2\ \mu\text{m}$ , respectively, and the wear track surface becomes smoother.

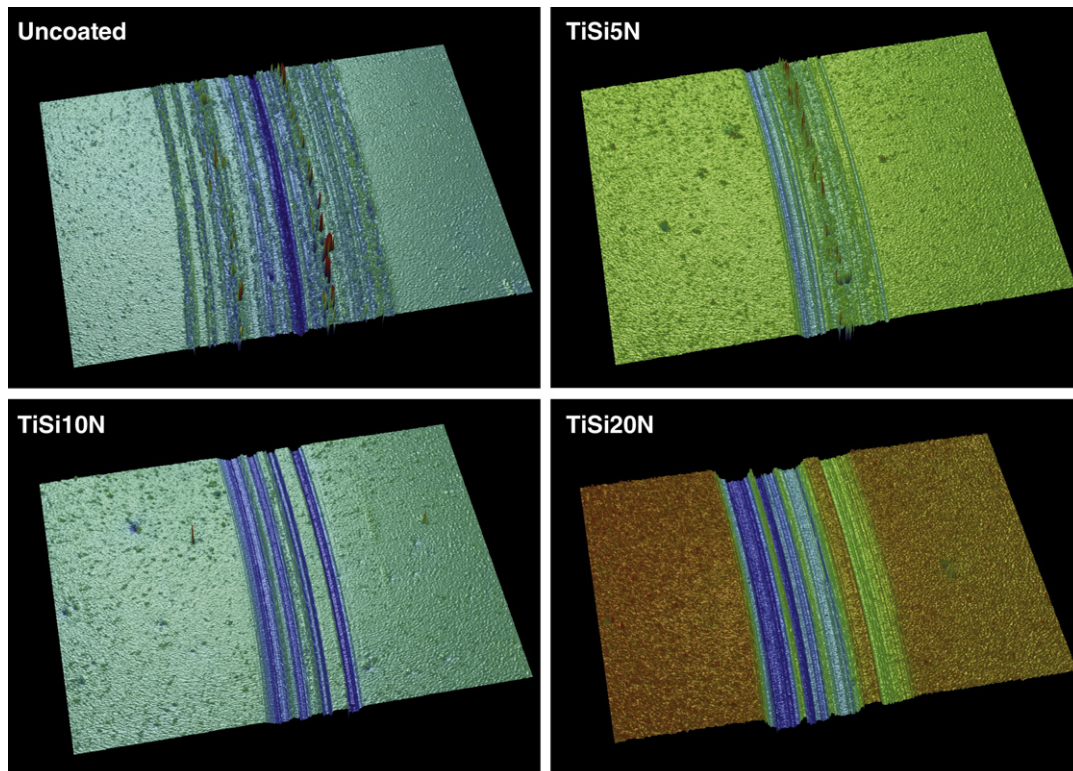


**Fig. 5.** Typical 3D images of the wear track on the uncoated, TiSi5N, TiSi10N, and TiSi20N coated 440a steel coupons tested against 302 SS balls at 1 N and 300 m.

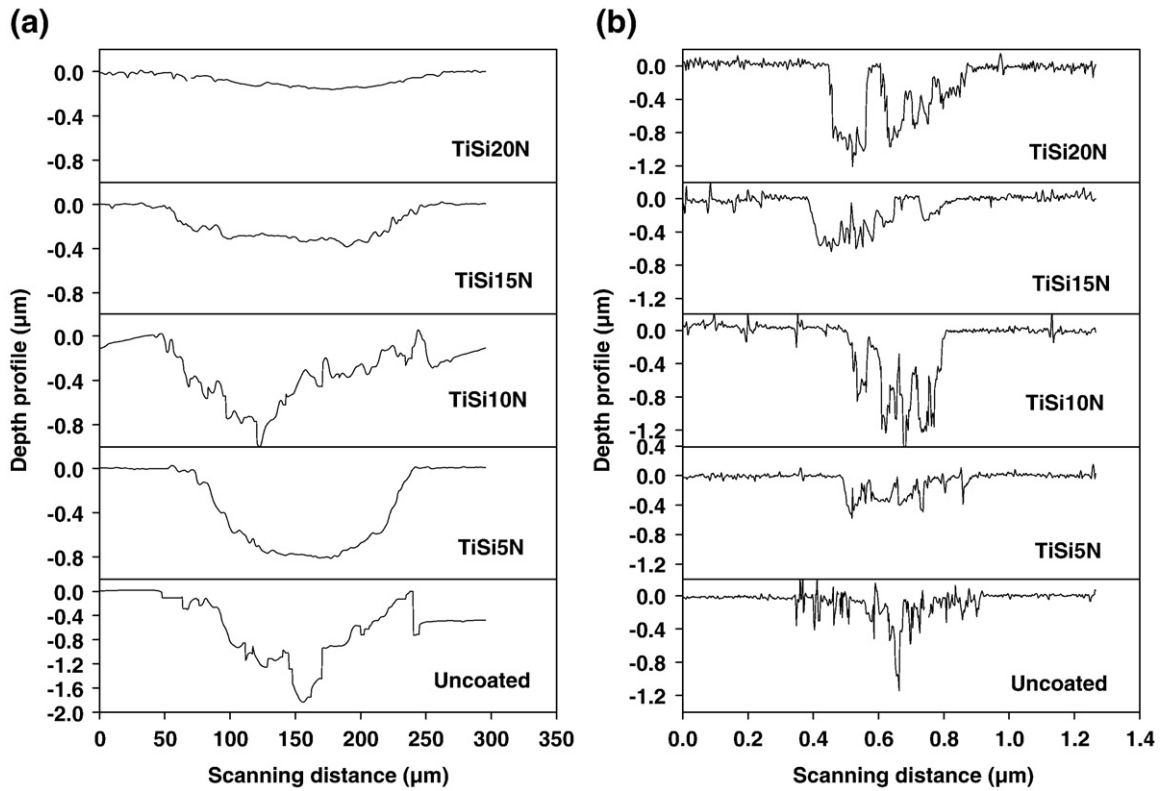


**Fig. 6.** Typical surface profiles of the wear track on the uncoated and TiSi5N, TiSi10N, TiSi15N, and TiSi20N coatings coated 440a stainless steel coupons tested against (a) Al<sub>2</sub>O<sub>3</sub> and (b) 302 stainless steel balls.

When 302 stainless steel balls were used, generally, the depth of the wear tracks is very shallow for all tested coupons. For the uncoated 440a coupons, the wear track is very wide and many spikes appear at the edges of the wear track. The spikes originated from the adhesion of the 302 stainless steel ball. Only very shallow (<0.4 µm) grooves are seen on the wear tracks of the TiN coated coupons. For the TiSi5N coated coupons, the depth of the wear track is also below 0.4 µm. With increasing Si content in the target to 10 at.%, the depth of the wear track increases to 0.8 µm. A further increase in the Si content in the coating results in a continuous increase in the depth, width, and the number of grooves in the wear track, indicating incorporation of Si into the coating leads to an increase in the wear rate.

Table 1 shows the calculated wear rate of the uncoated and TiSiN coated 440a stainless steel coupons against Al<sub>2</sub>O<sub>3</sub> and 302 stainless steel balls as well as the wear rate of the corresponding balls. When Al<sub>2</sub>O<sub>3</sub> balls were used, the uncoated steel substrate measured a fairly high wear rate of  $1.8 \times 10^{-5} \text{ mm}^3/\text{Nm}$ . The wear rate ( $0.97 \times 10^{-5} \text{ mm}^3/\text{Nm}$ ) reduces by 50% after coated with TiSi5N. With the increase of Si content in the coatings up to 7.7 at.%, the wear rate decreases continuously to  $1.40 \times 10^{-6} \text{ mm}^3/\text{Nm}$ , which is one order of magnitude lower than the uncoated coupons. It is observed that the wear rate of the Al<sub>2</sub>O<sub>3</sub> balls is very low for all the tests, but the wear rate of the Al<sub>2</sub>O<sub>3</sub> balls was significantly reduced when wear tested against TiSiN coated coupons. The coatings with higher Si content resulted in less wear of the Al<sub>2</sub>O<sub>3</sub> balls.

When wear tested against 302 stainless steel balls, due to the high hardness of the 440a stainless steel coupons, the uncoated coupons exhibited a low wear rate ( $1.13 \times 10^{-5} \text{ mm}^3/\text{Nm}$ ). However, the 302 stainless steel balls exhibited a high wear rate of  $1.15 \times 10^{-5} \text{ mm}^3/\text{Nm}$  due to the adhesion wear. The disk wear rate reduced slightly to  $8.6 \times 10^{-6} \text{ mm}^3/\text{Nm}$ , for the TiSiN coatings with Si content of 0.5 at.%, and the ball wear rate reduced by 75%. The further increase in the Si content in the TiSiN coatings to 7.7 at.% results in a continuous increase in the disk wear rate to  $3.63 \times 10^{-5} \text{ mm}^3/\text{Nm}$ , which is about 2 times higher than that of the uncoated coupons.

**4. Discussion**

Friction and wear performances of coatings are not inherent properties of the coating themselves. Instead, they are strongly dependent on the mechanical, chemical, and physical properties of the mating materials as well as their surface conditions.

Friction is the resistance to motion when two bodies in contact are forced to move relative to each other. Generally, the force of friction consists of two components: force to shear adhesion and force to plough the asperities on one surface through the other [28]. As most of the surfaces are rough on a micro or nano scale, only the tips of their asperities will contact when two surfaces are placed in contact. For clean surfaces, the atoms on one surface will attract those on the other and produce strong adhesion, which prevents the sliding of one

**Table 1**  
Wear rate of the coating and the balls after wear tests.

Ball materials		Uncoated	TiSi5N	TiSi10N	TiSi15N	TiSi20N
Al <sub>2</sub> O <sub>3</sub>	Disk wear rate, mm <sup>3</sup> /Nm	$1.83 \times 10^{-5}$	$9.74 \times 10^{-6}$	$7.25 \times 10^{-6}$	$3.43 \times 10^{-6}$	$1.40 \times 10^{-6}$
	Ball wear rate, mm <sup>3</sup> /Nm	$4.17 \times 10^{-7}$	$9.49 \times 10^{-8}$	$2.98 \times 10^{-7}$	$8.25 \times 10^{-8}$	$4.45 \times 10^{-8}$
302 SS	Disk wear rate, mm <sup>3</sup> /Nm	$1.13 \times 10^{-5}$	$8.61 \times 10^{-6}$	$1.87 \times 10^{-5}$	$1.58 \times 10^{-5}$	$3.63 \times 10^{-5}$
	Ball wear rate, mm <sup>3</sup> /Nm	$1.15 \times 10^{-5}$	$2.84 \times 10^{-6}$	$1.89 \times 10^{-6}$	$2.51 \times 10^{-6}$	$3.39 \times 10^{-6}$

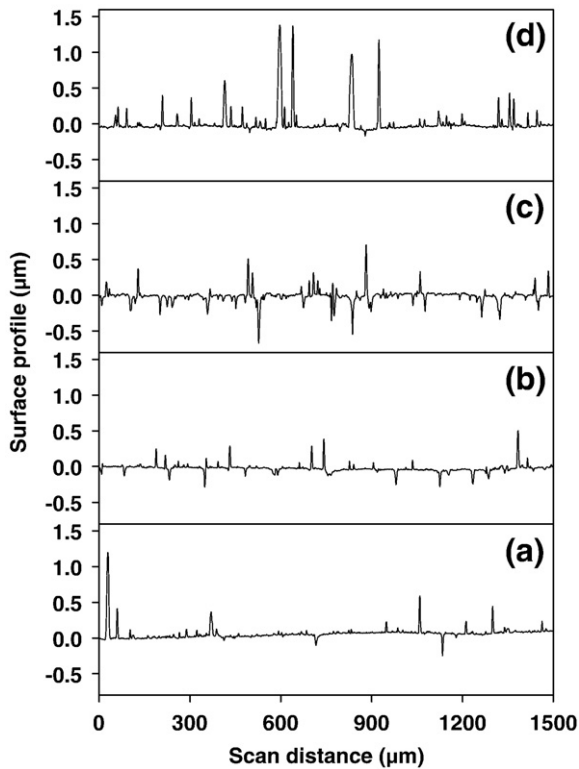


Fig. 7. Surface profiles of (a) TiSi5N, (b) TiSi10N, (c) TiSi15N, and (d) TiSi20N coated 440a coupons.

surface over the other and contributes to the first cause of friction. The asperities on the harder surfaces will plough out grooves in the softer surface, which constitutes the second cause of friction. On the uncoated 440a stainless steel, the local high temperatures generated by friction tends to soften and/or melt the asperities on the coupon

surface, leading to the cold welding of these asperities to the  $\text{Al}_2\text{O}_3$  and 302 stainless steel balls. This corresponds to the high friction coefficient of the uncoated 440a coupons when sliding against  $\text{Al}_2\text{O}_3$  and 302 stainless steel balls. When 440a coupons were coated with hard TiSiN coatings, the high melting point of both TiSiN coatings and  $\text{Al}_2\text{O}_3$  balls made the cold welding mechanism less important. In addition, the maximum Si content in the TiSiN coatings is only 7.7 at.%, the change in the chemical attractions between the Ti, Si, and N atoms in TiSiN coatings and the Al and O atoms in  $\text{Al}_2\text{O}_3$  ball with increasing Si content is also insignificant. In this case, the change in the surface roughness of the TiSiN coatings plays an important role to the friction.

Surface profilometer was used to characterize the surface roughness of the TiSiN coated 440a coupons. Fig. 7 depicts the typical surface profiles of the (a) TiSi5N, (b) TiSi10N, (c) TiSi15N, and (d) TiSi20N coated 440a coupons. Clearly, there are some spikes on all coating surfaces. With the increase in the Si content in the coatings, the density and height of the spikes increase continuously. The root-mean-square (RMS) surface roughness of the TiSi5N, TiSi10N, TiSi15N, and TiSi20N coatings was calculated. It was found that the RMS roughness of the TiSiN coatings increases monotonically from 38 to 63 nm with increasing Si content in the coatings from 0.5 to 7.7 at.%. As filtered cathodic arc technique could not remove 100% of the macro-particles, a small fraction of macro-particles will be condensed to the coating surface, corresponding to the formation of spikes as shown in Fig. 7. During the deposition of TiSiN coatings, for the targets with higher Si content, the arc plasma is less stable and tends to produce more macro-particles. As a result, more macro-particles were condensed on the coating surface for the coatings with higher Si content, corresponding to the formation of rougher surface. The increase in the surface roughness of TiSiN coatings with increasing Si content in the coatings may contribute to the increase in the friction coefficient as shown in Fig. 3.

Furthermore, the formation of a transfer layer on the ball surface plays a very important role in the friction process [29]. Optical microscopy was used to observe the surface morphology of the wear

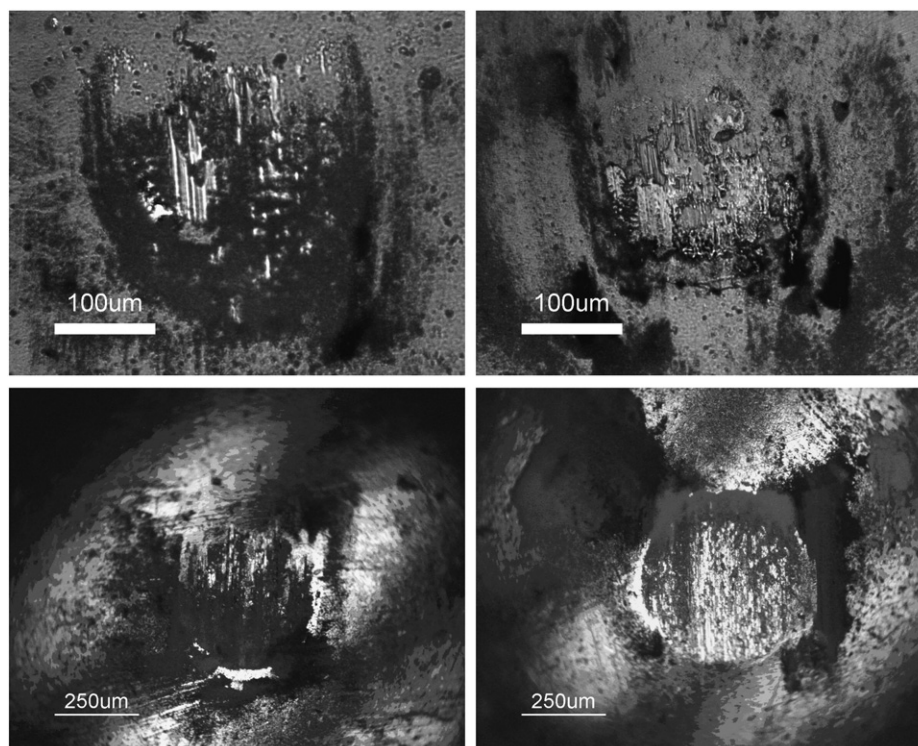


Fig. 8. Wear scar on  $\text{Al}_2\text{O}_3$  balls tested against (a) TiSi10N and (b) TiSi20N coatings, and on 302 stainless steel balls when tested against (c) TiSi10N and (d) TiSi20N coatings.

scar on the ball surface. Fig. 8 shows the optical images (20×) of the wear scar on Al<sub>2</sub>O<sub>3</sub> and 302 stainless steel balls tested against TiSi10N and TiSi20N coatings. As shown, for the TiSiN coatings with low Si content, part of the wear scar surface of both Al<sub>2</sub>O<sub>3</sub> and 302 stainless steel balls was covered with wear debris. This formed a loosely packed transfer layer on the wear scar surface. However, when tested against coatings with high Si content, the surface coverage area of the ball wear scar with wear debris became smaller. These observations indicate that for the coating with low Si content, the wear pairs change from TiSiN/Al<sub>2</sub>O<sub>3</sub> and TiSiN/302 stainless steel to TiSiN/TiSiN transfer layer. As the transfer layer was loosely packed, the wear debris on the transfer layer surface became free to slide and roll during wear testing, which significantly reduces the friction force and corresponds to a low friction coefficient. The coatings with high Si content lack the transfer layer, which corresponds to the large friction coefficient.

It is interesting to note that with increasing Si content in the coatings, the wear rate of the coatings decrease when tested against Al<sub>2</sub>O<sub>3</sub> balls and increases when tested against 302 stainless steel balls. The change in the wear rate for different TiSiN coatings also results from the formation of the transfer layer on the ball surface. When Al<sub>2</sub>O<sub>3</sub> balls were used, the wear mechanism for the TiSiN coatings was abrasive wear. In this case, the coating hardness plays a major role in the wear behavior. The hardness results show that the increase in the Si content in the coatings result in a continuous increase in hardness, corresponding to the monotonic decrease in the wear rate.

When 302 stainless steel balls were used during the wear test, the asperities on the coating surface were forced into soft 302 stainless steel balls, leading to wear of the 302 stainless steel balls. At the same time, 302 stainless steel balls exert strong shear force to the asperities, leading to the breakage of the asperities and formation of wear debris. This super-hard wear debris acts as abrasion media during the wear test, leading to the abrasive wear of the TiSiN coatings. Fig. 8 shows that transfer layers formed on the ball wear scar surface when worn against coatings with low Si content. The wear pairs change to TiSiN coatings against transfer layer. With the increase in the Si content in the coatings, less transfer layer formed on the ball wear scar surface. 302 stainless steel balls have more opportunity to directly rub against TiSiN coatings. The hard wear debris was pressed and embedded into the steel ball surface during testing, forming a composite surface layer consisting of super-hard TiSiN wear debris and tough 302 stainless steel. In this case, the embedded TiSiN wear debris was not free to move during testing, and acts as a cutting edge, leading to the formation of deep plough like grooves as shown in Fig. 6. This corresponds to the high wear rate of the TiSiN coatings with high Si content.

## 5. Conclusion

In this study, the mechanical properties, friction and wear performances of the TiSiN nanocomposite coatings with a thickness of 2.5 μm deposited using LAFAD technology were characterized by nanoindentation and pin-on-disk tribometer. Al<sub>2</sub>O<sub>3</sub> and 302 stainless steel balls were used as counterparts. Nanoindentation results show that the increase in the Si content in the TiSiN coatings leads to a continuous increase in the hardness and Young's modulus to 51 GPa and 449 GPa, respectively. Wear test results indicate that TiSiN coatings significantly reduce the wear rate and friction coefficient of

the 440a coupons. The tribological behaviors of the TiSiN coatings are strongly dependent on the Si content in the coatings and the ball material. TiSiN coatings exhibit similar friction coefficient when tested against Al<sub>2</sub>O<sub>3</sub> and 302 stainless steel balls, but the friction coefficient of the TiSiN coatings increases from 0.6 to 0.9 with increasing Si content in the coatings from 0.5 to 7.7 at.%, which resulted from the increase in the surface roughness with increasing Si content in the coating. With increasing Si content in the coatings from 0.5 to 7.7 at.%, the wear rate of the TiSiN coatings decrease from  $0.97 \times 10^{-5} \text{ mm}^3/\text{Nm}$  to  $1.40 \times 10^{-6} \text{ mm}^3/\text{Nm}$  when tested against Al<sub>2</sub>O<sub>3</sub> balls, but increases significantly from  $8.6 \times 10^{-6} \text{ mm}^3/\text{Nm}$  to  $3.63 \times 10^{-5} \text{ mm}^3/\text{Nm}$  when tested against 302 stainless steel balls. No significant change in the wear rate of the balls with Si content in the coatings is demonstrated.

## Acknowledgments

The authors would like to express gratitude for the support of The United States Army Telemedicine and Advanced Technology Research Center (TATRC), U.S. Army Medical Research & Materiel Command under contract number of W81XWH-08-2-0023.

## References

- [1] S. Veprek, M.G.J. Veprek-Heijman, Surf. Coat. Technol. 201 (2007) 6064.
- [2] S. Veprek, A. Niederhofer, K. Moto, T. Bolom, H.-D. Mannling, P. Nesladek, G. Dollinger, A. Bergmaier, Surf. Coat. Technol. 133–134 (2000) 152.
- [3] S. Veprek, M.G.J. Veprek-Heijman, P. Karvankova, J. Prochazka, Thin Solid Films 476 (2005) 1.
- [4] M. Diserens, J. Patscheider, F. Levy, Surf. Coat. Technol. 121 (1999) 158.
- [5] P.J. Martin, A. Bendavid, Surf. Coat. Technol. 163 (2003) 245.
- [6] J. Musil, J. Vlcek, Surf. Coat. Technol. 142–144 (2001) 557.
- [7] P. Steyer, A. Mege, D. Pech, C. Mendibide, J. Fontaine, J.F. Pierson, C. Esnouf, R. Goudeau, Surf. Coat. Technol. 202 (2008) 2268.
- [8] K.H. Kim, B.H. Park, Chem. Vapor Depos. 5 (1999) 275.
- [9] S.R. Choi, I.W. Park, S.H. Kim, K.H. Kim, Thin Solid Films 447–448 (2004) 371–376.
- [10] R. Wei, Surf. Coat. Technol. 2003 (2008) 538.
- [11] J.L. He, C.K. Chen, M.H. Hon, Wear 181–183 (1995) 189.
- [12] E. Varesi, G. Pavia, A. Zenkevich, Y. Lebedinskii, P. Besana, A. Giussani, A. Modelli, J. Phys. Chem. Solids 68 (2007) 1046.
- [13] J. Perez-Mariano, K.H. Lau, A. Sanjurjo, J. Caro, D. Casellas, C. Colominas, Surf. Coat. Technol. 201 (2006) 2217.
- [14] J.B. Choi, K. Cho, M.H. Lee, K.H. Kim, Thin Solid Films 447–448 (2004) 365.
- [15] M. Nose, Y. Deguchi, T. Mae, E. Honbo, T. Nagae, K. Nogi, Surf. Coat. Technol. 174 (2003) 261.
- [16] S.H. Kim, J.W. Jang, S.S. Kang, K.H. Kim, J. Mater. Process. Technol. 130–131 (2002) 283.
- [17] D.V. Shtansky, I.V. Lyasotsky, N.B. D'yakonova, F.V. Kiryukhantsev-Korneev, S.A. Kulnich, E.A. Levashov, J.J. Moore, Surf. Coat. Technol. 182 (2004) 204.
- [18] C.T. Guo, D. Lee, P.C. Chen, Appl. Surf. Sci. 254 (2008) 3130.
- [19] S.M. Yang, Y.Y. Chang, D.Y. Lin, D.Y. Wang, W. Wu, Surf. Coat. Technol. 202 (2008) 2176.
- [20] C.L. Chang, J.H. Chen, P.C. Tsai, W.Y. Ho, D.Y. Wang, Surf. Coat. Technol. 203 (2008) 619.
- [21] Y.H. Cheng, T. Browne, B. Heckerman, J. Vac. Sci. Technol., A 27 (2009) 82.
- [22] D. Ma, S. Ma, K. Xu, Vacuum 79 (2005) 7.
- [23] Flink, T. Larsson, J. Sjolen, L. Karlsson, L. Hultman, Surf. Coat. Technol. 200 (2005) 1535.
- [24] K.H. Kim, S.R. Choi, S.Y. Yoon, Surf. Coat. Technol. 298 (2002) 243.
- [25] J. Patscheider, T. Zehnder, M. Diserens, Surf. Coat. Technol. 146–147 (2001) 201.
- [26] Y.H. Cheng, T. Browne, B. Heckerman, J.C. Jiang, E.I. Meletis, C. Bowman, V. Gorokhovskiy, J. Appl. Phys. 104 (2008) 093502.
- [27] Y.H. Cheng, T. Browne, B. Heckerman, J.C. Jiang, E.I. Meletis, C. Bowman, V. Gorokhovskiy, J. Phys., D. Appl. Phys. 42 (2009) 125,415.
- [28] M.J. Neale, The Tribology Handbook, Butterworth-Heinemann, Oxford, 1995.
- [29] L. Wang, X. Nie, J. Housden, E. Spain, J.C. Jiang, E.I. Meletis, A. Leyland, A. Matthews, Surf. Coat. Technol. 203 (2008) 816.